Long range correlation of molecular orientation and vibration in liquid $CDCl_3$

Cite as: AIP Advances 12, 105008 (2022); doi: 10.1063/5.0107226
Submitted: 7 July 2022 • Accepted: 15 September 2022 •
Published Online: 20 October 2022

David P. Shelton[a]

AFFILIATIONS

Department of Physics and Astronomy, University of Nevada, Las Vegas, Nevada 89154-4002, USA

[a]Author to whom correspondence should be addressed: shelton@physics.unlv.edu

ABSTRACT

The polarization dependence of hyper-Rayleigh second harmonic light scattering (SHS) and hyper-Raman light scattering (HRS) measured for liquid $CDCl_3$ show the effect of long-range correlation of molecular orientation and vibration. HRS from the ν_1, ν_4, and ν_5 vibration modes is polarized transverse to the scattering wavevector, whereas HRS from the ν_2, ν_3, and ν_6 vibration modes and SHS from the ν_0 orientation mode all show longitudinal polarization. The transverse polarized HRS is accounted for by long range vibration correlation due to dipole–dipole interaction for molecules at 20–400 nm separation. Longitudinal SHS and HRS are due to the combined effect of long range dipole–dipole orientation correlation and the increment in the molecular first hyperpolarizability induced by short range intermolecular interactions.

I. INTRODUCTION

Long range orientation correlation in liquids has received renewed recent interest since it was shown that second harmonic light scattering (SHS or hyper-Rayleigh scattering) provides a method to measure the long range molecular orientation correlation in polar liquids.[1–10] Long range orientation correlation with the form of a solenoidal vector field, mediated by the dipole–dipole interaction in polar liquids, was theoretically predicted long in advance of the measurements.[11,12] Such solenoidal long range molecular orientation correlation produces SHS that is polarized transverse to the scattering vector. However, results of some recent SHS experiments for several molecules have found longitudinal polarized SHS,[1,10] in disagreement with this theoretical prediction. It is unclear how to account for such longitudinal SHS, and it was proposed that short range steric interactions may produce long range orientation correlation opposite to the theoretical prediction.[1]

Hyper-Raman scattering (HRS), which has been used to investigate phonon modes in crystals, can also probe the long range correlation of molecular vibration in molecular liquids.[13] The propagating phonons in crystals are the result of short range interactions and have transverse or longitudinal polarization with respect to the wavevector of the phonon. Such transverse and longitudinal nonlocal vibration modes, where vibration is correlated over distances comparable to the wavelength of the scattering wavevector, have been found in several glasses and molecular liquids including CCl_4.[13–16] Recent HRS measurements also found long range correlation of the molecular vibrations in CCl_4 and conclude that this is due to the long range dipole–dipole interaction between transition dipoles.[16]

The present work applies the SHS measurement techniques and analysis used in previous studies of long range orientation correlation in liquids to the study of orientation and vibration correlation in liquid $CDCl_3$.[6,16,17] Local modes and nonlocal transverse and longitudinal modes are distinguished by the polarization dependence of SHS or HRS for the mode.[18] The SHS or HRS scattering configurations with the incident and scattered light polarized either perpendicular or parallel to the horizontal scattering plane are denoted VV, HV, VH, and HH, where V denotes vertical polarization, H denotes horizontal polarization, and the first and second letters refer to the incident and scattered light, respectively. At 90° scattering angle, the SHS or HRS intensity ratio I_{HV}/I_{VH} for a polar mode is I_{HV}/I_{VH} = 1, 2, or 0 according to whether the mode is local, transverse, or longitudinal. The experimental study below presents SHS and HRS spectral measurements for liquid $CDCl_3$ in four linear polarization configurations. The measurements are combined to decompose the spectrum into local, transverse, and longitudinal components, and the results are interpreted in terms of a dipole–dipole correlation model.

II. EXPERIMENT

The experiment measures scattered light that is Raman-shifted from the laser second harmonic frequency. Linearly polarized pulses from an injection-seeded, cavity-dumped, single longitudinal mode Nd:YAG (yttrium aluminum garnet) laser (operating at $\lambda = 1064$ nm, 10 kHz repetition rate, 6 ns pulse duration, 100 MHz linewidth) are focused to a 8 μm diameter beam waist in the liquid sample in a standard square 10 mm fluorimeter cuvette. The average laser power was about 2 W, and to avoid breakdown at the focus, dust was removed from the $CDCl_3$ sample by continuous flow in a closed loop containing the sample cell and a 0.2 μm PTFE (polytetrafluoroethylene) filter. Scattered light at $\theta = 90°$ was collected and collimated by an aspheric lens ($f = 4$ mm), analyzed by a linear polarizer, focused into an optical fiber, and fiber-coupled to the spectrometer and photon counting detector. The background count rate of the gated photomultiplier was 0.0010 s^{-1}. The sample cell temperature was 25 °C for all measurements. $CDCl_3$ rather than $CHCl_3$ was chosen to minimize laser beam absorption and thermal lensing effects. The temperature increase at the beam waist in the $CDCl_3$ sample is 0.5 °C, based on beam propagation and thermal analysis similar to that for CH_3CN where absorption is 24 times larger.[19,20]

A scanning grating spectrometer was used to measure the SHS and HRS spectrum and also to measure the SHS or HRS intensity at selected fixed frequencies. The spectral slit width was 12 cm^{-1} [full width at half maximum (FWHM)] for most measurements. Multiple scans were averaged to eliminate the effect of laser power fluctuation and drift during the measurements. Spectra for polarization analysis were acquired from sequential scans with VV, HH, VH, and HV polarization, repeated up to 2000 times, and summed for each polarization configuration.

The spectrometer response has strong polarization dependence, so an effective depolarizer is required between the analyzing polarizer and the spectrometer. The combination of a long multimode fiber (40 m) followed by a liquid crystal polymer microarray depolarizer was used. The polarization response of the system was calibrated using a thermal light source and an integrating sphere placed at the sample position.

The SHS or HRS intensity ratios I_{VV}/I_{HV}, I_{HV}/I_{VH}, and I_{HH}/I_{VH} at several fixed frequencies selected by the spectrometer were also accurately measured using techniques previously described.[17] Several hundred alternate 10 s measurements of the two polarization configurations for each ratio are averaged to cancel the effect of intensity fluctuation and drift. Rapid switching between

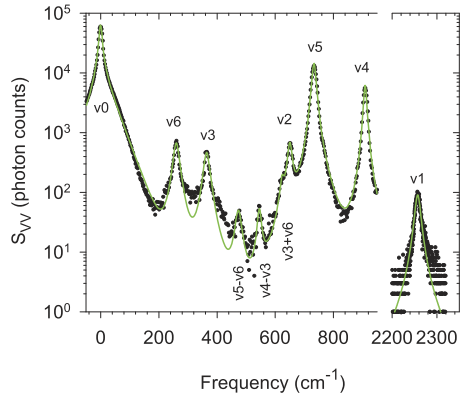

FIG. 1. VV SHS and HRS spectrum of $CDCl_3$ scanned with 12 cm^{-1} spectral resolution, showing data points and fitted curve. Frequency ν is the Stokes Raman shift.

TABLE I. Peak positions, widths (FWHM), and normalized integrated intensities for the VV SHS and HRS spectrum in Fig. 1.

Mode	Species	Position (cm^{-1})	Width (cm^{-1})	Intensity
ν_0	A_1	0	20	1000
ν_6	E	260	24	14
ν_3	A_1	364	24	10
ν_5-ν_6	$A_1 + A_2 + E$	473	24	1.0
ν_4-ν_3	E	545	15	0.6
ν_3+ν_6	E	624	16	1.6
ν_2	A_1	650	17	9
ν_5	E	733	16	207
ν_4	E	909	12	64
ν_1	A_1	2257	14	4.4

TABLE II. SHS and HRS polarization ratios for $CDCl_3$ measured at frequency shift ν with 12 cm^{-1} spectral resolution, at 90° scattering angle and extrapolated to zero collection aperture.

Mode	ν (cm^{-1})	I_{VV}/I_{HV}	I_{HV}/I_{VH}	A_T/A_0	A_L/A_0	A_L/A_T
ν_0	0[a]	3.49 ± 0.02	0.864 ± 0.003	0.361 ± 0.005	0.780 ± 0.013	2.16 ± 0.05
ν_0	0	2.672 ± 0.005	0.896 ± 0.001	0.185 ± 0.001	0.460 ± 0.004	2.49 ± 0.02
ν_0	0[b]	2.586 ± 0.004	0.929 ± 0.002	0.169 ± 0.006	0.349 ± 0.004	2.06 ± 0.02
ν_0	80	3.95 ± 0.06	1.050 ± 0.008	0.48 ± 0.02	0.34 ± 0.03	0.70 ± 0.06
ν_6	260	6.01 ± 0.06	0.908 ± 0.013	1.51 ± 0.05	2.02 ± 0.10	1.34 ± 0.08
ν_3	363	5.52 ± 0.07	0.809 ± 0.012	1.16 ± 0.04	2.17 ± 0.10	1.88 ± 0.11
ν_2	651	6.23 ± 0.07	0.661 ± 0.009	1.71 ± 0.07	4.49 ± 0.18	2.63 ± 0.15
ν_5	733	8.20 ± 0.02	1.808 ± 0.007	8.39 ± 0.25	0.00 ± 0.05	0.00 ± 0.01
ν_4	909	8.31 ± 0.03	1.834 ± 0.013	9.92 ± 0.45	−0.01 ± 0.09	0.00 ± 0.01
ν_1	2257	5.49 ± 0.08	1.175 ± 0.022	1.14 ± 0.05	0.50 ± 0.08	0.44 ± 0.07

[a] 2 cm^{-1} FWHM resolution.
[b] 60 cm^{-1} FWHM resolution, from Ref. 10.

polarization configurations was done using a liquid crystal variable wave plate to control the laser polarization and a fast rotator to control the analyzing polarizer for the scattered light. The collection numerical aperture (NA) was controlled by a circular aperture following the collection lens. Except for the VV SHS and HRS survey spectrum with NA = 0.50, spectra were scanned with NA = 0.12 and corrected for the effect of the finite collection aperture. The corrections are obtained by numerically integrating over the collection aperture using expressions from Ref. 21 and validated by measurements over a range of NA extrapolated to NA = 0.[17]

III. EXPERIMENTAL RESULTS

The VV SHS and HRS spectrum measured for $CDCl_3$ is shown in Fig. 1, and the peak fit parameters for this spectrum are given in Table I. SHS and HRS polarization ratios measured at scattering angle $\theta = 90^\circ$, at the positions of the fundamental peaks, are given in Table II.

The SHS or HRS intensities due to the octupolar contribution A_0, the dipolar transverse mode contribution A_T, and the dipolar longitudinal mode contribution A_L, assuming Kleinman symmetry, are[18]

$$I_{VV} = (3/2)A_0 + 9A_T, \tag{1}$$

$$I_{HV} = A_0 + A_T, \tag{2}$$

$$I_{HH} = I_{VH} = A_0 + (1/2)(A_T + A_L), \tag{3}$$

where $I_{VV}/I_{HV} = 3/2$ for pure octupolar SHS or HRS (third rank irreducible spherical tensor part of the molecular first hyperpolarizability tensor β) and $I_{VV}/I_{HV} = 9$ for pure dipolar SHS or HRS (first rank irreducible spherical tensor part of β).[13,15,22]

The SHS or HRS intensity ratios measured with VV, HV, and VH linear polarization configurations are combined to determine the octupolar mode, polar transverse mode, and polar longitudinal mode contributions using the following relations,

$$A_0 = (6/5)I_{HV} - (2/15)I_{VV}, \tag{4}$$

$$A_T = (2/15)I_{VV} - (1/5)I_{HV}, \tag{5}$$

$$A_L = (2/15)I_{VV} - (11/5)I_{HV} + 2I_{VH}, \tag{6}$$

with the results for A_T/A_0, A_L/A_0, and A_L/A_T given in Table II. Long range correlation for a mode is indicated by deviation from $A_L/A_T = 1$ for that mode. All the modes in Table II show significant long range correlation. The results $A_L/A_T = 0$ for ν_4 and ν_5 indicate that they are nearly pure transverse vibration modes. The ν_1 vibration is also transverse, while ν_2, ν_3, and ν_6 are longitudinal. The ν_0 orientation mode of the SHS spectrum is longitudinal at the band center but becomes transverse in the wings. The octupolar contribution is larger than the dipolar contributions for the SHS ν_0 orientation mode, but the reverse is the case for all the HRS vibration modes.

Figures 2–4 show the VV, HH, VH, and HV spectra acquired for the ν_0 and ν_5 bands. These data are combined to calculate the A_0, A_T, and A_L spectra, point by point, using Eqs. (4)–(6). The A_0, A_T, and A_L spectra for the ν_0 orientation mode are fit with the sum of a clipped Lorentzian function and an exponential function,

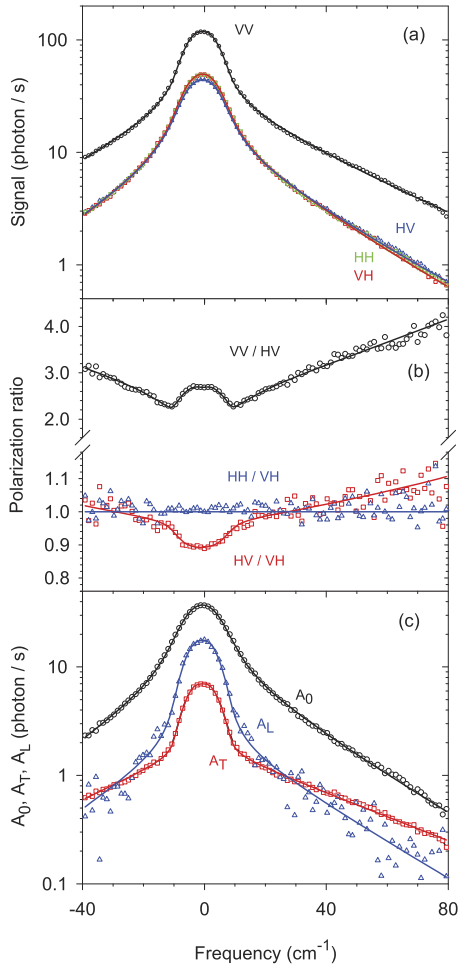

FIG. 2. (a) SHS spectra for the ν_0 mode scanned with 12 cm^{-1} resolution, showing data points measured with four linear polarization configurations. Data points obtained by combining the data at each frequency are shown for (b) the polarization ratios and (c) the intensities A_0, A_T, and A_L. The functions fit using the combined data in Figs. 2 and 3 are shown by the solid curves.

$$I(\Delta\nu) = [I_1(\Delta\nu) + I_2(\Delta\nu)]\exp(-\Delta\nu/2kT), \tag{7}$$

$$I_1(\Delta\nu) = 2A_1[1 + \exp|\Delta\nu/\Delta\nu_0|]^{-1}[1 + (\Delta\nu/\Delta\nu_1)^2]^{-1}, \tag{8}$$

$$I_2(\Delta\nu) = A_2\ \exp(-|\Delta\nu/\Delta\nu_2|), \tag{9}$$

where $\Delta\nu = (\nu - \tilde{\nu}_j)$ for mode ν_j. The Lorentzian function in Eq. (8) has its far wings clipped by the exponential factor with $\Delta\nu_0 = 90\ cm^{-1}$ to account for non-diffusive reorientation on time scales < 0.05 ps. The exponential function in Eq. (9) represents the prominent collision induced exponential wing extending 200 cm^{-1} from the line center on the SHS profile. The final exponential factor in Eq. (7)

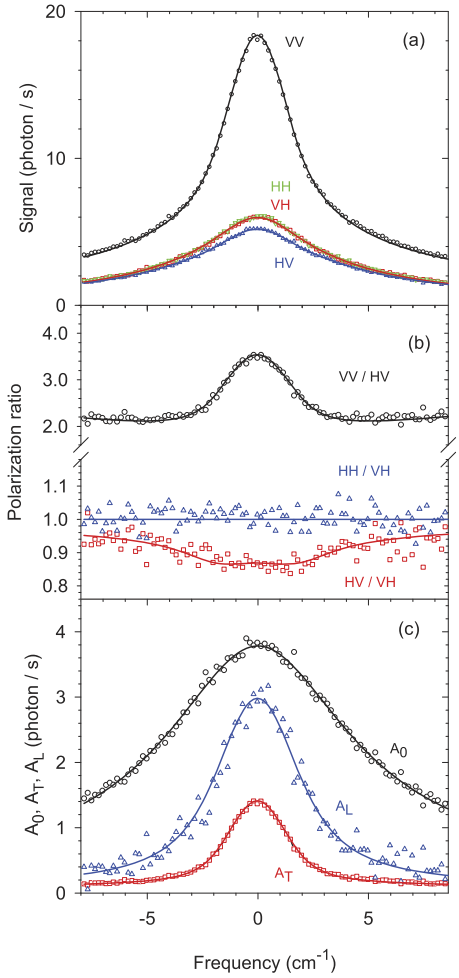

FIG. 3. (a) SHS spectra for the ν_0 mode scanned with 2 cm^{-1} resolution, showing data points measured with four linear polarization configurations. Data points obtained by combining the data at each frequency are shown for (b) the polarization ratios and (c) the intensities A_0, A_T, and A_L. The functions fit using the combined data in Figs. 2 and 3 are shown by the solid curves.

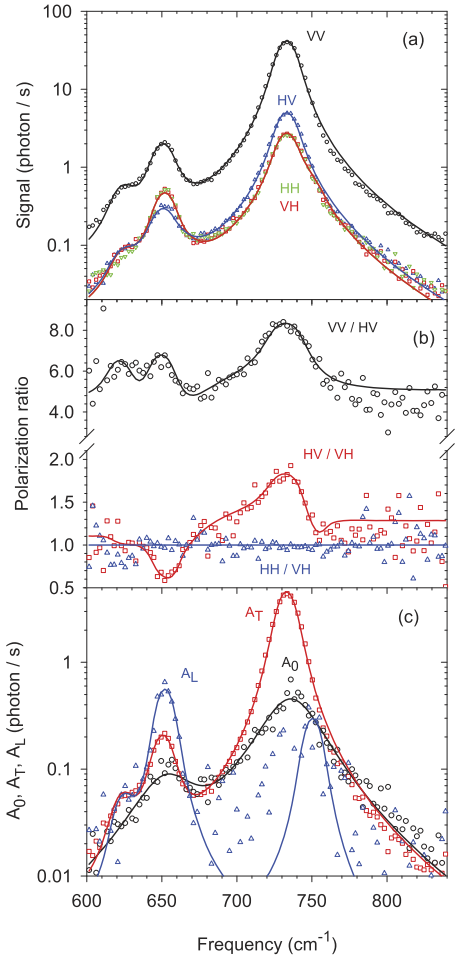

FIG. 4. (a) HRS spectra for the ν_5, ν_2, and $\nu_3 + \nu_6$ modes, showing data points measured with four linear polarization configurations. Data points obtained by combining the data at each frequency are shown for the (b) polarization ratios and (c) the intensities A_0, A_T, and A_L. The function fit to the combined data is shown by the solid curves.

accounts for the Stokes/anti-Stokes asymmetry (2 kT = 414 cm^{-1} at 25 °C). The function obtained as the convolution of $I(\Delta\nu)$ with the spectrometer transmission function is fit to the A_0, A_T, and A_L data in Figs. 2 and 3, with the fit parameters A_1, $\Delta\nu_1$, A_2/A_1, and $\Delta\nu_2$ given in Table III (the A_1 values for Fig. 2 are 13.3 times larger). The fitted curves in Figs. 2(a), 2(b), 3(a), and 3(b) are obtained from the fitted curves shown in Figs. 2(c) and 3(c) using Eqs. (1)–(3). The A_0, A_T, and A_L curves are all centered at $\tilde{\nu}_0 = 0$ cm^{-1} but differ in width.

Rotational diffusion of a symmetric top molecule produces a Lorentzian line shape with a width proportional to $J(J+1)$ for the multipolar contribution of rank J.[23] This rotational diffusion model predicts that the octupolar spectral width is 6 times larger than the dipolar spectral width, as compared with the ratio 5.2 for the measured A_0 and A_T Lorentzian widths in Table III. From the 2.7 cm^{-1} Raman spectral width measured at 300 K for $CHCl_3$ one estimates 0.9 cm^{-1} for the dipolar HRS spectral width,[24] close to the measured width 0.94 cm^{-1} for the A_T Lorentzian. The A_L width is 1.9 times larger, which is not consistent with dipolar rotational diffusion and needs an explanation.

The broad exponential wing of the SHS spectrum is due to the short lived transient increment $\Delta\beta$ induced in a molecule by the rapidly varying octupolar electric field of a neighbor molecule during a close collision. This contribution was previously investigated

TABLE III. Fit parameters for the spectra in Figs. 2 and 3.

Mode	A_1 (s^{-1})	$\Delta\nu_1$ (cm^{-1})	A_2/A_1	$\Delta\nu_2$ (cm^{-1})
A_0	3.08(2)	4.85(4)	0.261(4)	22.8(1)
A_T	1.84(2)	0.94(1)	0.071(1)	36.0(2)
A_L	3.25(9)	1.80(7)	0.058(4)	23.6(12)

TABLE IV. Fit parameters for the ν_5, ν_2, and $\nu_3 + \nu_6$ spectra in Fig. 4.

Mode	$\bar{\nu}_j$ (cm^{-1})	A_1 (s^{-1})	$\Delta\nu_1$ (cm^{-1})
A_0	736.0(6)	0.48(2)	21.8(9)
	653(2)	0.076(6)	21.8
A_T	733.05(2)	6.13(2)	5.97(2)
	650.5(1)	0.251(4)	5.97
	623.7(4)	055(2)	5.97
A_L	751(1)	0.46(7)	4.2
	652.1(4)	0.88(8)	4.2(5)
	624	0.06(2)	4.2

using SHS in CCl_4 and $CDCl_3$.[16,23,25] The most recent SHS investigation for CCl_4 found transverse polarization of the exponential wing, which was explained by correlation of $\Delta\beta$ due to the interaction of the transient dipoles also induced during these close collisions.[16] This can also account for the transverse polarization of the SHS wing for $CDCl_3$.

Figure 4 shows the spectral region containing the ν_5, ν_2, and $\nu_3 + \nu_6$ vibration modes. The data for A_T are fit by the sum of three clipped Lorentzian functions with the form given by Eq. (8) and the same width, convolved with the spectrometer transmission function. The data for A_0 and A_L are also fit with similar functions, giving the fit parameters in Table IV and the fitted curves plotted in Fig. 4. The weak A_L component for the ν_5 vibration at 751 cm^{-1} is shifted 18 cm^{-1} from the A_T component at 733 cm^{-1} and has peak intensity 0.075 times that of the A_T peak, much larger than the intensity ratio at 733 cm^{-1} reported in Table II. The A_L peak at 751 cm^{-1} in Fig. 4(c) is a good fit to the data despite the appearance; the points on the low frequency side of the peak are scattered evenly around zero intensity but the negative excursions are not visible due to the logarithmic scale. The A_T-A_L splitting for ν_5 is analogous to the transverse-longitudinal frequency splitting for phonons in crystals. No splitting is observed for the weaker ν_2 vibration at 650 cm^{-1}.

IV. DIPOLE CORRELATION

Long range orientation correlation of $CDCl_3$ molecules detected by the SHS measurements is thought to be the result of the dipole–dipole interaction, but to make a quantitative comparison with the SHS measurements, the required calculations need the orientation correlation function over the full range of intermolecular distances. A molecular dynamics (MD) simulation has been done to compute the dipole correlation function for liquid $CDCl_3$ at short to intermediate distances, in order to assess its contribution to the SHS results. The simulation for $CDCl_3$ [Optimized Potentials for Liquid Simulations (OPLS) all atom force field, GROMACS-2021.2] with 8000 molecules in a 10.17 nm box was equilibrated for 0.5 ns before a 10 ns production run with 2 fs time steps.

The full, longitudinal, and transverse dipole–dipole correlation functions computed from the simulation trajectory are[6]

$$F(r) = \langle \hat{\mu}_i \cdot \hat{\mu}_j \rangle, \tag{10}$$

$$L(r) = \langle (\hat{\mu}_i \cdot \hat{r}_{ij})(\hat{\mu}_j \cdot \hat{r}_{ij}) \rangle, \tag{11}$$

TABLE V. Summary of MD simulation results for $CDCl_3$.

Parameter	Value	Expt. value[28]	Units
ρ	7.602	7.504	nm^{-3}
μ	1.467[a]		D
y	0.555		
g_K	1.337		
ϵ	4.020	4.806	
a^3	9.505		10^{-3} nm^3

[a] 4.893×10^{-30} C m.

$$T(r) = (1/2)[F(r) - L(r)], \tag{12}$$

where $\hat{\mu}_i$ is the dipole unit vector on molecule i and $\hat{r}_{ij}$ is the unit vector in the direction from molecule i to j. Corrections $\delta F = 3\delta L = 3\delta T = -(\epsilon - 1)^2/(9y\epsilon_0 k_B T)$ are added to the MD simulation results for F, L, T to obtain results for an infinite homogeneous system from the results obtained using periodic boundary conditions,[7,26,27] where

$$y = \rho\mu^2/(9\epsilon_0 k_B T) \tag{13}$$

is the dimensionless dipole strength, ρ is the molecular number density, and μ is the molecular dipole moment.[6] The dielectric constant ϵ is calculated using the correlation function expression

$$g_K = 1 + 4\pi\rho \int_0^\infty F(r) g(r) r^2 \, dr \tag{14}$$

for the Kirkwood correlation factor g_K and then solving the Kirkwood relation

$$(\epsilon - 1)(2\epsilon + 1)/\epsilon = 9yg_K \tag{15}$$

for ϵ.[6] The correlation functions at large r for a non-polarizable dipole fluid have the asymptotic values

$$L(r) = -2T(r) = a^3/r^3 \tag{16}$$

with the correlation strength parameter[6]

$$a^3 = (\epsilon - 1)^2/(18\pi y\epsilon\rho). \tag{17}$$

MD simulation results for $CDCl_3$ are summarized in Table V, and the correlation functions are shown in Fig. 5. The radial pair distribution function $g(r)$ plotted in Fig. 5(a) shows that other molecules are excluded for $r < 0.27$ nm. The r^3-weighted correlation functions plotted in Fig. 5(c) reach constant long range limiting values for $r > 3$ nm, with limiting values in good agreement with the values calculated using Eqs. (16) and (17). Also plotted in Fig. 5 are the correlation functions,

$$B_{Lm}(r) = [1 + (r/a)^2]^{-3/2}[1 - (3/2)r^2/(r^2 + a^2)], \tag{18}$$

$$B_{Tm}(r) = [1 + (r/a)^2]^{-3/2}, \tag{19}$$

for a model solenoidal vector field with $a^3 = 9.5 \times 10^{-3}$ nm^3, which matches the asymptotic form of the MD simulation results.

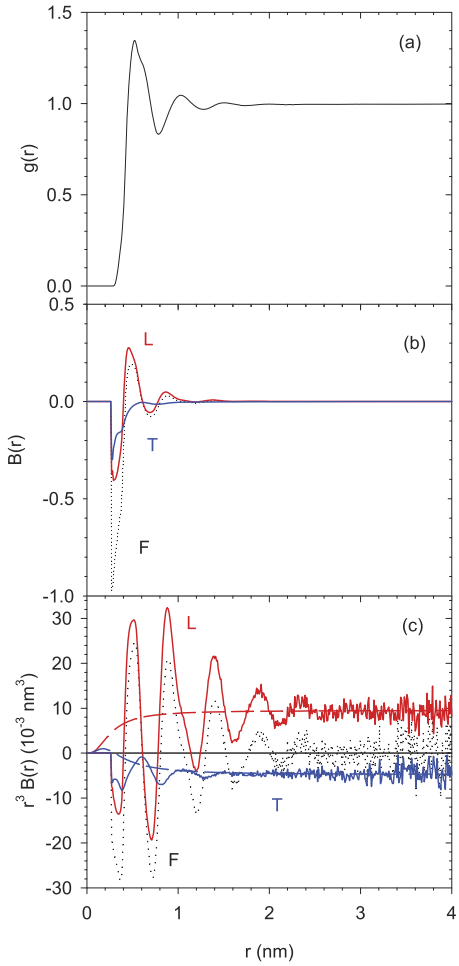

FIG. 5. MD simulation results for (a) the radial pair distribution function $g(r)$ and (b) and (c) the dipole correlation functions $B(r)$, where $B = F$ (dotted black), L (solid red), T (solid blue), B_{Lm} (dashed red), and B_{Tm} (dashed blue), are given by Eqs. (10)–(12), (18), and (19), respectively.

The MD simulation results can be used to calculate the intensities A_T and A_L for dipolar orientation SHS including the effects of short and long range correlation. The intensities A_T and A_L are proportional to the diagonal components $S_T(K)$ and $S_L(K)$ of the spatial Fourier transform of the dipole correlation tensor, given by the expressions[6–8]

$$S_T(K) = 4\pi \int_0^\infty \left\{ B_T(r)\left[j_0(Kr) - \frac{j_1(Kr)}{Kr}\right] + B_L(r)\frac{j_1(Kr)}{Kr} \right\} g(r) r^2\, dr, \tag{20}$$

$$S_L(K) = 4\pi \int_0^\infty \left\{ B_L(r)\left[j_0(Kr) - \frac{2j_1(Kr)}{Kr}\right] + B_T(r)\frac{2j_1(Kr)}{Kr} \right\} g(r) r^2\, dr, \tag{21}$$

where $B_T(r)$ and $B_L(r)$ are the diagonal components of the correlation tensor and $j_n(x)$ are the spherical Bessel functions.

These integrals are evaluated piecewise over three regions,

$$S_T = S_{T,1} + S_{T,2} + S_{T,3}, \tag{22}$$

$$S_L = S_{L,1} + S_{L,2} + S_{L,3}. \tag{23}$$

Region 1 is the excluded volume for $r < r_1 = 0.27$ nm, region 2 is the intermediate zone $r_1 < r < r_2$, and region 3 is asymptotic zone $r > r_2 = 3.0$ nm.

The delta function self-correlation in region 1 gives

$$S_{T,1} = S_{L,1} = (1/3)(4\pi r_0^3/3), \tag{24}$$

where $4\pi r_0^3/3 = \rho^{-1}$ is the volume per molecule.

At short range, in region 2 where $Kr \ll 1$, it is a good approximation to take the $K = 0$ limit for the integrand in Eqs. (20) and (21). Using the correlation functions from the MD simulation, this gives

$$S_{T,2} = S_{L,2} = 4\pi \int_{r_1}^{r_2} [L(r) + 2T(r)] g(r) r^2\, dr. \tag{25}$$

At long range, in region 3, the integrals in Eqs. (20) and (21) are evaluated with $g(r) = 1$ and the correlation functions $B_{Tm}(r)$ and $B_{Lm}(r)$ from Eqs. (18) and (19). Integrating and then taking the $K = 0$ limit gives

$$S_{T,3} = 2\pi a^3 - S_{TL,3}, \tag{26}$$

$$S_{L,3} = 0 - S_{TL,3}, \tag{27}$$

where

$$S_{TL,3} = 4\pi \int_0^{r_2} [B_{Lm}(r) + 2B_{Tm}(r)] g(r) r^2\, dr = (4\pi a^3/3)[1 + (a/r_2)^2]^{-3/2}. \tag{28}$$

The results for $S_T(K)$ and $S_L(K)$ obtained using Eqs. (22)–(28) are given in Table VI. The difference between $S_T(K)$ and $S_L(K)$ arises from the integration over the range $0.5 < Kr < 10$, where K is the scattering wavevector (see Fig. 4 of Ref. 7). The $K = 0$ limit for the integrals is a good approximation provided that $Ka \ll 1$. In the present experiment, $a \approx 0.21$ nm, $K^{-1} \approx 42$ nm, and $Ka \approx 0.005$. The integration range $0.5 < Kr < 10$, where the observed difference

TABLE VI. Dipolar HRS calculated using MD for $CDCl_3$.

Parameter	Value	Units (nm^3)
$S_{T,1} = S_{L,1}$	43.85	10^{-3}
$S_{T,2} = S_{L,2}$	44.29	10^{-3}
$S_{TL,3}$	39.52	10^{-3}
$2\pi a^3$	59.72	10^{-3}
S_T	108.34	10^{-3}
S_L	48.62	10^{-3}
S_L/S_T	0.449	

between S_T and S_L is produced by the correlations, corresponds to intermolecular distances 21 nm < r < 420 nm. The MD simulation predicts transverse HRS with $A_L/A_T = S_L/S_T = 0.449$, and the theory for a non-polarizable dipole fluid predicts that the long range dipole–dipole correlation will always result in $S_L < S_T$. This does not agree with the observed longitudinal HRS with $A_L/A_T = 2.16$ for ν_0 in Table II.

V. LONGITUDINAL SHS

The outstanding unexplained fact is the observed longitudinal SHS for the ν_0 orientation mode. Theory that considers just dipole–dipole correlation for the permanent molecular dipole and vector β predicts transverse SHS and cannot account for longitudinal SHS. A possible resolution is a contribution from a different correlation. To search for a correlation that can produce the observed longitudinal SHS, rotational invariants can be used to express all orientation correlations with different angular dependence that can contribute to SHS for an isotropic liquid. The rotational invariant expansions for the VV, HV, VH, and HH SHS intensities at 90° scattering angle are given in the Appendix for molecules with C_{2v} or C_{3v} symmetry, where one sees that only dipolar and octupolar correlations can contribute to SHS. By inspection of the terms in these expansions, one can effectively rule out octupolar orientation correlation contributions producing the observed longitudinal SHS. The argument is as follows.

Long range dipole correlation produces $I_{HV}/I_{VH} > 1$ and $I_{HH}/I_{VH} = 1$ due to the terms with negative h^{112}, where $h^{112}(K = 0) = -(\epsilon - 1)^2/3y\epsilon$. A sufficiently large negative coefficient h^{332} (or positive h^{334}) could reduce the ratio I_{HV}/I_{VH} to agree with the observed value for ν_0, but the ratio I_{HH}/I_{VH} would increase by the same amount. No such deviation from $I_{HH}/I_{VH} = 1$ is seen in Figs. 2–4. The value $I_{HH}/I_{VH} = 1.000 \pm 0.001$ was measured for ν_0 (at $\nu = 0$ cm^{-1} with 12 cm^{-1} resolution, $\theta = 90°$, NA = 0) in the present experiment, and the result 0.999 ± 0.002 was previously measured.[10] This rules out any significant ν_0 SHS contribution due to octupolar long range orientation correlation for $CDCl_3$.

Based on $A_L/A_T = 0.449$ from the MD simulation, one expects to find an A_L peak in Fig. 3(c) with the same width and 0.45 times the amplitude of the A_T peak. A revised fit to the A_L data, using the sum of a fit function with the original form and a 0.45× scaled A_T peak function, gives an equally good fit to the data with parameters $A_1 = 2.57 \pm 0.08$ and $\Delta\nu_1 = 1.96 \pm 0.09$ for the excess A_L Lorentzian peak. It appears that the A_L peak for ν_0 is the sum of at least two different contributions, where the excess A_L component has an integrated intensity larger than A_T.

Excess longitudinal SHS due to dissolved ions is ruled out since small ions are nearly insoluble in $CDCl_3$ due to the low dielectric constant, and since the spectral width of an ion-induced signal would be < 0.001 cm^{-1}.[29] Previous high spectral resolution SHS measurements for $CDCl_3$ are consistent with zero ion-induced SHS.[10]

The discussion above has considered SHS mediated by a constant molecular hyperpolarizability β tensor, identical on each molecule, and has neglected the effect of the molecular environment on β. The sum of multipole electric fields E from neighboring molecules will induce an increment $\Delta\beta = \gamma E$ on each molecule, where γ is the molecular second hyperpolarizability. Induced $\Delta\beta$ accounts for about half the SHS intensity for liquid CCl_4,[25] and a similar large contribution for $CDCl_3$ may be expected. Below it is shown that longitudinal SHS is produced when $\Delta\beta$ and its correlation are included in the analysis.

The SHS contribution that is altered by dipole correlation is that due to $\beta_\parallel$, the vector component of β in the direction of the molecular dipole. This $\beta_\parallel$ is measured by electric-field-induced second harmonic generation (EFISH or ESHG) experiments. Gas phase ESHG for $CHCl_3$ and $CDCl_3$ gives $\beta_\parallel = 1 \pm 3$ and 1 ± 4 a.u.,[30] as compared with -4 ± 1 a.u. from an *ab initio* calculation where convergence was carefully investigated.[31] Liquid phase ESHG gives $\beta_\parallel = -68 \pm 7$ a.u.,[32] while $|\beta_\parallel| = 11 \pm 1$ is estimated from SHS.[23] Atomic units (a.u.) for β and γ are β(a.u.) = $\beta(3.206\,361 \times 10^{-53}$ C^3 m^3 J$^{-2})$ and γ(a.u.) = $\gamma(6.235\,377 \times 10^{-65}$ C^4 m^4 J$^{-3})$.[33] Despite absolute calibration problems for the liquid measurements, both experiments show larger $\beta_\parallel$ for molecules in the liquid, and the sign of $\beta_\parallel$ is negative.

For each molecule in the liquid, the component of the fluctuating electric field due to neighbor molecules has a non-zero average projection along the molecular dipole axis because of the orientation correlation of the molecules. The average electric field component along the dipole axis of a molecule due to the surrounding molecular dipoles is

$$\langle E_z \rangle \le 4\pi\rho \int \frac{2\,\mu}{4\pi\epsilon_0 r^3} F(r) g(r) r^2\, dr, \tag{29}$$

and the field calculated using the MD simulation results for $CDCl_3$ is $\langle E_z \rangle = 1.93 \times 10^8$ V/m. The sign of the average field is positive, so with $\gamma = 11.6 \pm 0.6 \times 10^3$ a.u. for $CDCl_3$,[30] the increment $\Delta\beta_\parallel = \gamma\langle E_z \rangle = 4.3$ a.u. induced by this field is also positive. There can be a non-zero contribution to $\langle E_z \rangle$ due to the surrounding molecular octupoles, but this contribution will be determined by correlations at a shorter range and with different angular dependence than the dipole contribution.

The dipolar SHS intensity due to permanent and fluctuating β of the molecules in the liquid is proportional to

$$\langle (\beta_\parallel + \Delta\beta_\parallel)_i (\beta_\parallel + \Delta\beta_\parallel)_j \rangle = \langle (\beta_\parallel)_i (\beta_\parallel)_j \rangle + 2\langle (\beta_\parallel)_i (\Delta\beta_\parallel)_j \rangle + \langle (\Delta\beta_\parallel)_i (\Delta\beta_\parallel)_j \rangle \tag{30}$$

averaged over all molecules i and j. The calculation in Sec. IV included short and long range correlations and addressed the term $\langle (\beta_\parallel)_i (\beta_\parallel)_j \rangle$ for molecules with constant β. The result $A_L \neq A_T$ is due to long range orientation correlations, which vary as r^{-3}. The long range correlation function for $(\beta_\parallel)_i$ is the same as for μ_i, whether $(\beta_\parallel)_i$ on each molecule is parallel to μ_i on that molecule, or is antiparallel to μ_i on each molecule. However, the long range correlation for $(\Delta\beta_\parallel)_i$ vanishes since the fluctuating field generating it is governed by $F(r)$. The term $\langle (\Delta\beta_\parallel)_i (\Delta\beta_\parallel)_j \rangle$ vanishes at long range since fluctuating fields on distant molecules are not synchronized; the $(\Delta\beta_\parallel)_i$ are not long range correlated because $F(r)$ is not. In contrast, the cross-term $2\langle (\beta_\parallel)_i (\Delta\beta_\parallel)_j \rangle$ does not vanish at long range because $(\Delta\beta_\parallel)_j$ is always aligned parallel with the permanent dipole μ_j, which is correlated at long range with μ_i and thus, $(\beta_\parallel)_i$.

For $CDCl_3$ the average $(\Delta\beta_\parallel)_i$ is parallel to μ_i, and $(\beta_\parallel)_j$ is antiparallel to μ_j, so the long range correlation for $(\Delta\beta_\parallel)_i$ and $(\beta_\parallel)_j$ is

the same as for μ_i and μ_j, but with the opposite sign. The correlation functions for the cross term contribution are the same $L(r)$ and $T(r)$ as in the last section, except with a minus sign because $\Delta\beta_\parallel$ and $\beta_\parallel$ have the opposite sign, so the cross term produces longitudinal HRS instead of transverse HRS.[8] The broader spectrum for A_L due to the cross term, as compared to the A_T spectrum, indicates that the time scale for the cage field fluctuations producing $\Delta\beta$ is shorter than the time scale for reorientation of β for the caged molecule. Both the negative $\beta_\parallel$ measured by liquid phase ESHG and the intensities $A_L > A_T$ measured by SHS from $CDCl_3$ can be obtained if $0.5 < -\Delta\beta_\parallel/\beta_\parallel < 1$. The result $A_L > A_T$ for orientation mode SHS is also found in several other liquids and can occur when $\beta_\parallel$ is negative and $0.5 < -\Delta\beta_\parallel/\beta_\parallel$.[1,10]

In summary, dipole–dipole correlation of molecules with constant β will result in transverse SHS, but longitudinal SHS can result when one includes the interference between permanent β on one molecule and induced $\Delta\beta$ on another. The widths of the transverse and longitudinal SHS spectra report the respective time scales for molecular reorientation and local field fluctuation.

VI. TRANSVERSE AND LONGITUDINAL HRS

The pattern of transverse and longitudinal HRS observed for the vibration modes can be understood using the analysis developed for longitudinal SHS. Three of the $CDCl_3$ vibration modes, ν_1, ν_4, and ν_5, exhibit transverse HRS and long range correlation that can be understood as the result of the dipole–dipole interaction.

The transition dipole for the ν_1 C-D symmetric stretching mode is parallel to the permanent dipole μ_0, so the ν_1 vibration transition dipoles inherit the orientation correlation of the permanent molecular dipoles. Table VII shows that the ν_1 transition dipole moment is 200 × smaller than the permanent dipole,[28,34,35] so orientation correlation is not significantly increased by the interaction between transition dipoles. The ratio $A_L/A_T = 0.44$ observed for the ν_1 mode is the same as the value 0.45 predicted using the MD simulation results for orientation correlation. The D motion during the C-D symmetric stretch will modulate the distance between the D atom and the surrounding molecules, inducing an increment $\Delta\beta$ oscillating at the vibration frequency, which is aligned along the molecular symmetry axis on average. This induced $\Delta\beta$ will not affect the result for A_L/A_T if $\Delta\beta$ has the same sign as transition β for the vibration, or has a much smaller magnitude.

TABLE VII. Gas phase permanent dipole[28] and vibration transition dipoles[34,35] for $CDCl_3$ in units of 10^{-30} C m.

Mode	Value	Deformation[35]
ν_0	3.37	
ν_1	0.015	C-D stretch
ν_2	0.178	C–Cl symmetric stretch
ν_3	0.073	C–Cl symmetric bend
ν_4	0.411	C–Cl antisymmetric stretch, C-D wag
ν_5	0.790	C–Cl antisymmetric stretch
ν_6	0.037	C–Cl asymmetric bend

The transition dipoles for the ν_4 and ν_5 modes of E symmetry are perpendicular to the permanent dipole axis, so the orientation correlation of μ_0 does not contribute to vibration correlation for these modes, but the transition dipoles are large enough that the resonant dipole–dipole coupling between the transition dipole moments on the vibrating molecules can account for the vibration correlation. The dipole produced by a linear combination of the twofold degenerate modes of E symmetry is free to point in any direction in the plane perpendicular to the molecular axis, so even the weaker coupling of the transition dipoles for these modes can produce the observed correlation. The anti-symmetry of the C–Cl stretching motions for these modes can result in canceling increments $\Delta\beta$ from the Cl atom interactions with the surrounding molecules, so one expects $|\Delta\beta| \ll |\beta|$ and transverse HRS as a result.

The ν_2, ν_3, and ν_6 vibration modes show longitudinal HRS. Longitudinal HRS can result if there is interference, similar to Eq. (30), between the vibration transition β and a correlated parallel increment $\Delta\beta$ oscillating at the vibration frequency but of the opposite sign.

Consider first the ν_2 and ν_3 modes with A_1 symmetry, where the transition β vector is aligned with the permanent dipole axis, so that it inherits the long range orientation correlation of the permanent molecular dipole. The Cl motion during the C–Cl symmetric stretch for the ν_2 vibration will modulate the distance between the Cl atoms and the surrounding molecules, inducing an increment $\Delta\beta$ oscillating at the vibration frequency, which is aligned along the molecular symmetry axis on average. Longitudinal HRS will result if this increment is of the opposite sign and $|\Delta\beta| > 0.5|\beta|$. For the ν_3 symmetric C–Cl bend mode, the Cl motion will produce a similar result.

The transition dipole for the ν_6 asymmetric C–Cl bending mode is perpendicular to the permanent dipole so the long range correlation of transition β for the vibration is due to the weak transition dipole–dipole interaction. Longitudinal HRS again requires an opposite sign $\Delta\beta$ increment with $|\Delta\beta| > 0.5|\beta|$.

Finally, $\Delta\beta$ induced by the rapidly varying octupolar electric field of colliding neighbor molecules during close collisions generates the broad spectral wing of the ν_0 mode.[16,23,25] The octupolar field induced effects for $CDCl_3$ are expected to be similar to those previously determined for CCl_4, with $\Delta\mu$ as large as the transition dipoles for the ν_4 and ν_5 modes of $CDCl_3$, and $\Delta\beta$ as large as the permanent β for $CDCl_3$.[16] Induced $\Delta\beta$ is correlated with induced $\Delta\mu$ and will experience the effect of the long range orientation correlation of induced $\Delta\mu$, produced by the dipole–dipole interaction. Transverse SHS is expected and observed for the ν_0 spectral wing. There will be no longitudinal SHS component due to interference between permanent β and $\Delta\beta$ for this intermolecular vibration, since there is little spectral overlap between the broad spectral wing and the narrow Lorentzian orientation peak.

VII. CONCLUSION

The polarization dependence of hyper-Raman scattering from liquid $CDCl_3$ provides evidence for long range correlation of molecular orientation and vibration in the liquid. Orientation correlation due to the dipole–dipole interaction between permanent or vibration transition dipoles, varying as r^{-3} at long range, can account for the observed transverse polarized HRS. The observed longitudinal polarized SHS and HRS can also be accounted for by the same

dipole orientation correlations when the effect of short range interactions and correlations acting to modify the hyperpolarizability of the molecules is included.

ACKNOWLEDGMENTS

This work was supported by the National Science Foundation under Award No. CHE-1953941.

AUTHOR DECLARATIONS

Conflict of Interest

The authors have no conflicts to disclose.

Author Contributions

David P. Shelton: Conceptualization (lead); Data curation (lead); Formal analysis (lead); Funding acquisition (lead); Investigation (lead); Methodology (lead); Project administration (lead); Resources (lead); Software (lead); Supervision (lead); Validation (lead); Visualization (lead); Writing – original draft (lead); Writing – review & editing (lead).

DATA AVAILABILITY

The data that support the findings of this study are available within the article.

APPENDIX: SHS ROTATIONAL INVARIANT EXPANSION

The first hyperpolarizability tensor $\beta_{\alpha\beta\gamma}$ in the static limit is symmetric in all indices, and this is often a good approximation at optical frequencies (Kleinman symmetry). In this case, β is the sum of irreducible spherical tensors of rank 1 and 3, with components $\beta_m^{[ss,J]}$ for $J = 1$ and 3.[22] Following Ref. 1 one may express the intensity for HRS using the rotational invariant expansion for the molecular pair correlation function with expansion coefficients $h^{l_1 l_2 l}(K)$, where $l_1 = l_2 = 1$ or 3, $0 \le l \le l_1 + l_2$, and l = even. The dipole correlation functions and the rotational invariant coefficients h^{11l} are related by $h^{110}(r) = F(r)$ and $h^{112}(r) = 2L(r) - 2T(r)$.[36] The rotational invariant expansions for the VV, HV, VH, and HH HRS intensities for 90° scattering angle are

$$I_{VV}/\kappa = \frac{9}{45}C_1 + \frac{6}{105}C_3 + \frac{1}{45}D_1[h^{110} - h^{112}] + \frac{2}{1715}D_3[h^{330} - h^{332} + 9h^{334} - 225h^{336}], \quad \text{(A1)}$$

$$I_{HV}/\kappa = \frac{1}{45}C_1 + \frac{4}{105}C_3 + \frac{1}{45}D_1\left[\frac{1}{9}h^{110} - \frac{1}{9}h^{112}\right] + \frac{2}{1715}D_3\left[\frac{2}{3}h^{330} - \frac{1}{4}h^{332} - \frac{113}{12}h^{334} + \frac{135}{4}h^{336}\right], \quad \text{(A2)}$$

$$I_{VH}/\kappa = \frac{1}{45}C_1 + \frac{4}{105}C_3 + \frac{1}{45}D_1\left[\frac{1}{9}h^{110} + \frac{1}{18}h^{112}\right] + \frac{2}{1715}D_3\left[\frac{2}{3}h^{330} - \frac{1}{2}h^{332} + h^{334} + \frac{225}{2}h^{336}\right], \quad \text{(A3)}$$

$$I_{HH}/\kappa = \frac{1}{45}C_1 + \frac{4}{105}C_3 + \frac{1}{45}D_1\left[\frac{1}{9}h^{110} + \frac{1}{18}h^{112}\right] + \frac{2}{1715}D_3\left[\frac{2}{3}h^{330} - \frac{3}{4}h^{332} + \frac{29}{4}h^{334} + \frac{585}{8}h^{336}\right], \quad \text{(A4)}$$

where

$$C_J = \Sigma_m|\beta_m^{[ss,J]}|^2, \quad \text{(A5)}$$

$$D_J = |\Sigma_m\beta_m^{[ss,J]}|^2. \quad \text{(A6)}$$

The non-vanishing, independent components of β for molecules with C_{2v} or C_{3v} symmetry and Kleinman symmetry are β_{zzz}, $\beta_{zxx} = u\beta_{zzz}$, $\beta_{zyy} = v\beta_{zzz}$, and $\beta_{yyy} = w\beta_{zzz}$, where $u = v$ for C_{3v} or $w = 0$ for C_{2v}, and the coefficients C_J and D_J are

$$C_1 = D_1 = \frac{3}{5}(1 + u + v)^2\beta_{zzz}^2, \quad \text{(A7)}$$

$$C_3 = \left[\frac{1}{10}(3u + 3v - 2)^2 + 4w^2\right]\beta_{zzz}^2, \quad \text{(A8)}$$

$$D_3 = \frac{1}{10}(3u + 3v - 2)^2\beta_{zzz}^2. \quad \text{(A9)}$$

REFERENCES

[1] J. Duboisset, F. Rondepierre, and P.-F. Brevet, J. Phys. Chem. Lett. **11**, 9869 (2020).
[2] J. Duboisset and P.-F. Brevet, Phys. Rev. Lett. **120**, 263001 (2018).
[3] D. Borgis, L. Belloni, and M. Levesque, J. Phys. Chem. Lett. **9**, 3698 (2018).
[4] L. Belloni, D. Borgis, and M. Levesque, J. Phys. Chem. Lett. **9**, 1985 (2018).
[5] Y. Chen, N. Dupertuis, H. I. Okur, and S. Roke, J. Chem. Phys. **148**, 222835 (2018).
[6] M. B. Rodriquez and D. P. Shelton, J. Chem. Phys. **148**, 134504 (2018).
[7] D. P. Shelton, J. Chem. Phys. **147**, 154501 (2017).
[8] D. P. Shelton, J. Chem. Phys. **143**, 134503 (2015); **146**, 199901 (2017).
[9] D. P. Shelton, J. Chem. Phys. **141**, 224506 (2014).
[10] D. P. Shelton, J. Chem. Phys. **136**, 044503 (2012).
[11] M. S. Wertheim, J. Chem. Phys. **55**, 4291 (1971).
[12] G. Stell, G. N. Patey, and J. S. Høye, Adv. Chem. Phys. **48**, 183 (1981).
[13] V. N. Denisov, B. N. Mavrin, and V. B. Podobedov, Phys. Rep. **151**, 1 (1987).
[14] B. Hehlen and G. Simon, J. Raman Spectrosc. **43**, 1941 (2012).
[15] V. Rodriguez, J. Raman Spectrosc. **43**, 627 (2012).
[16] D. P. Shelton, J. Chem. Phys. **154**, 034502 (2021).
[17] D. P. Shelton, Rev. Sci. Instrum. **82**, 113103 (2011).
[18] D. P. Shelton, J. Opt. Soc. Am. B **17**, 2032 (2000); **34**, 1550 (2017).
[19] R. D. Pyatt and D. P. Shelton, J. Chem. Phys. **114**, 9938 (2001).
[20] J. P. Gordon, R. C. C. Leite, R. S. Moore, S. P. S. Porto, and J. R. Whinnery, J. Appl. Phys. **36**, 3 (1965).
[21] D. P. Shelton, J. Chem. Phys. **132**, 154506 (2010).
[22] P. D. Maker, Phys. Rev. A **1**, 923 (1970).
[23] P. Kaatz and D. P. Shelton, Opt. Commun. **157**, 177 (1998).
[24] W. G. Rothschild, R. M. Cavagnat, and P. Maraval, J. Chem. Phys. **99**, 8922 (1993).
[25] P. Kaatz and D. P. Shelton, Mol. Phys. **88**, 683 (1996).
[26] V. Ballenegger and J.-P. Hansen, Mol. Phys. **102**, 599 (2004).

[27]J. M. Caillol, J. Chem. Phys. **96**, 7039 (1992).
[28]R. C. Weast, *CRC Handbook of Chemistry and Physics*, 68th ed. (CRC, Boca Raton, 1987).
[29]D. P. Shelton, J. Chem. Phys. **130**, 114501 (2009).
[30]P. Kaatz, E. A. Donley, and D. P. Shelton, J. Chem. Phys. **108**, 849 (1998).
[31]F. D. Vila, D. A. Strubbe, Y. Takimoto, X. Andrade, A. Rubio, S. G. Louie, and J. J. Rehr, J. Chem. Phys. **133**, 034111 (2010).
[32]F. Kajzar, I. Ledoux, and J. Zyss, Phys. Rev. A **36**, 2210 (1987).
[33]D. P. Shelton and J. E. Rice, Chem. Rev. **94**, 3 (1994).
[34]D. M. Bishop and L. M. Cheung, J. Phys. Chem. Ref. Data **11**, 119 (1982).
[35]J. Morcillo, J. F. Biarge, J. M. V. Heredia, and A. Medina, J. Mol. Struct. **3**, 77 (1969).
[36]J.-P. Hansen and I. R. McDonald, *Theory of Simple Liquids*, 4th ed. (Academic, 2013).